Chapter 6
Electron Beam Generation and Experimental Results

6.1 Introduction

Performance of the electron beam and radiation generated at the SURIYA facility depends critically on the RF-gun operation. After the RF-gun was installed in the beamline, high RF-power operation has been applied to determine the RF-pulse width and its level that is sufficient to generate an electron beam with the desired properties. During this thesis project most effort was spent on early stages of the SURIYA system including the electron beam characterization at the exit of the RF-gun. However, some parameters of the electron beam after the linac acceleration will be presented in order to described the beam parameters for the transition radiation.

6.2 RF-Gun Setup and Conditioning

An RF-gun was installed as an electron source of the SURIYA beamline in March 2003. Special care of cleanliness is required during the gun installation. An introduction of dust, oil or foreign material into the RF-gun and vacuum component surfaces must be avoided. Since the RF-gun is required to be in a ultra high vacuum environment three ion pumps are connected to the RF-gun and its RF-input waveguide to maintain a good vacuum at the RF-gun. The average base pressure of the RF-gun at room temperature without RF-power but open to the beam line with an α-magnet chamber is $2-3\times10^{-8}$ Torr and comes down to $1-2\times10^{-9}$ Torr when the gun valve is closed. Since the thermionic cathode is very sensitive to poor vacuum when it is hot the vacuum in the RF-gun must be kept in the order of 10^{-8} Torr or below.

6.2.1 Gun Temperature Control

Due to thermal expansion, the cavity radius changes and hence the resonant frequency when the temperature of the RF-cavity changes. To simplify the

relation between the resonant frequency and the cavity temperature, the resonant frequency of the TM_{010}-mode pillbox cavity with the cavity radius a in vacuum can be written as

$$f_0 = \frac{2.405c}{2\pi a}. \tag{6.1}$$

By differentiating (6.1) with respect to the temperature T, we get a relation of frequency change with temperature change as

$$\frac{\Delta f_0}{\Delta T} = -\frac{2.405c}{2\pi a^2}\frac{\Delta a}{\Delta T} = -\frac{2.405c}{2\pi a^2}a_0\alpha \approx -\frac{2.405c}{2\pi a}\alpha, \tag{6.2}$$

where α is the thermal coefficient of expansion, which in case of copper $\alpha = 16.9\times10^{-6}$ $^oC^{-1}$ [50]. The variation of the cavity radius is very small, then the final cavity radius (a) is close to the original radius (a_0) and we can set $a_0 \approx a$. The scaling law in (6.2) can be used to estimate the frequency change due to temperature for copper RF-cavities operating in TM_{010}-mode. For the 2856 MHz pillbox cavity of radius is 4.02 cm, the resonant frequency of the cavity will decrease while the temperature increase as -48.3 kHz/^{o}C. Hence, the RF-gun must be temperature stabilized and a water cooling circuit made of copper tube is therefore brazed to the outside surface of the gun to keep the gun body at a constant temperature.

A controllable water cooling/heating system has been installed and connected to the gun copper cooling tube. Copper is a more preferable material for using as the cooling tube than ion or stainless steel due to its high thermal conductivity. The RF-gun temperature was monitored by an electrical sensor circuit at the gun external surface. The sensor can measure temperature range of -50 to 150 ^{o}C. The incoming water temperature becomes stable when the temperature of the sensor reaches the temperature set point. The temperature of the gun body can be set between 20 to 100 ^{o}C and can be maintained within $\pm0.5^oC$ from the set point. This temperature variation leads to the resonant frequency change of $\pm$25 kHz. From the low power RF-measurement results in Chapter 4, the temperature of the gun body is chosen to operated at 27.5 ^{o}C yielding a frequency of 2856 MHz in the RF-gun operation.

6.2.2 Vacuum Baking

There are two processes to be performed before the RF-gun functions as an electron sources in normal operation. First, the RF-gun requires a low

temperature vacuum bake after it is installed in the beamline in order to clean up the gun surface. Second, an RF-processing or an RF-training of the RF-gun, without the cathode heater on, is needed to reach RF-power levels sufficiently high to produce an electron beam with the desired properties. These processes including the cathode processing are necessary only once unless the RF-gun is exposed to a poor vacuum or a chemical contamination happens.

The RF-gun baking was performed by wrapping the gun body including the rectangular waveguide and the vacuum manifold with heating tape and covering all components with aluminum foil to contain the heat and maintain a uniform baking temperature. The gun temperature was monitored continuously with the temperature sensor at the gun body surface after the heating tape was turned on. The temperature of the gun was slowly raised to about 100°C, while keeping the vacuum pressure below 10^{-6} Torr. It should be noted that the best baking temperature is about 200°C. However, at that high temperature the temperature sensor cannot function due to its limitation. The RF-gun was baked for about 24 hours until the pressure was in the 10^{-8} Torr range. Then, the heating tape was turned off after cool down of the the RF-gun to room temperature RF-processing was performed.

6.2.3 RF-Gun Conditioning and Breakdown Phenomena

Internal surfaces of the RF-gun will outgas in the presence of high RF-fields. Instant application of very high RF-power might cause electrical breakdown of a ceramic RF-window and discharges in the gun cavity. The RF-gun had to be processed or trained, before it could function as an electron emitter, by slowly increasing the RF-power from low RF-level with short RF-pulse width while the cathode heater was off. RF-conditioning is required to clean the dust or contaminant material on the gun surface. The number of electrons and ions emitted from the gun surface depends on its structure shapes and surface conditions. The maximum accelerating field gradient of the RF-gun is limited by this outgassing. In addition, the electrons and ions can cause a break down phenomenon resulting in the shortening of the cathode lifetime due to excessive pressure inside the RF-gun. The maximum RF-power the the gun can handle is limited by breakdown phenomenon. The reflected RF-signal was observed to monitor for breakdown or

arcing in the RF-gun. When the breakdown happened all RF-power is reflected from the gun for a short moment.

At SURIYA, the RF-gun processing was started from 2.4 MW with an RF-pulse width of about 2 μs (FWHM). Its amplitude was raised to a maximum value before the pulse width was increased. Increasing in both the RF-level and the RF-pulse width results in higher average power as can be calculated from (5.5). If the vacuum pressure jumps above 10^{-7} Torr or any arc in the gun and waveguide system was monitored during the RF-conditioning, the RF-power is reduced or shut off immediately. After continuous RF-processing for several days, the RF-gun reached the maximum RF-power of about 5.2 MW with 6 μs (FWHM) at 10 Hz for several hours without sparking or breakdown. The base pressure of the RF-gun of about 5×10^{-8} Torr, before conditioning began, rose to a maximum of 7×10^{-8} Torr during the RF-conditioning. After the RF-processing was completed the base pressure at the RF-gun decreased to about 1.9×10^{-8} Torr without RF-power and about 3×10^{-8} at normal operation with the RF-power and hot cathode.

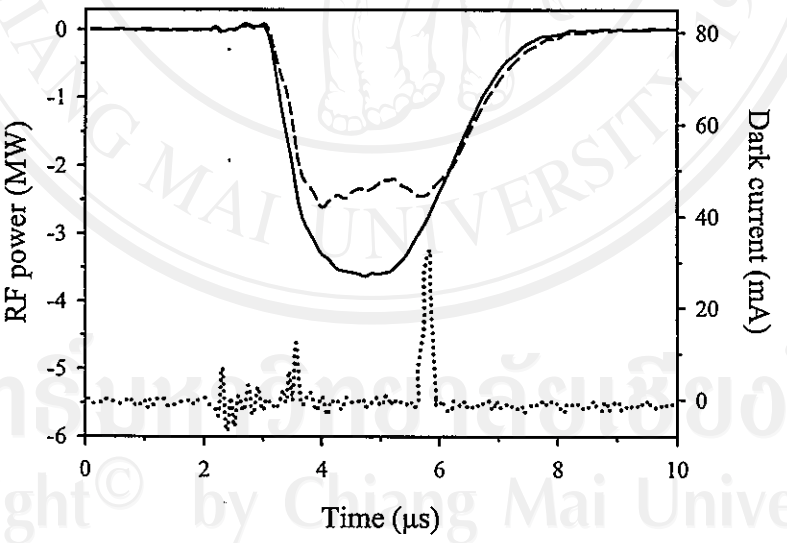

Figure 6.1. Forward (solid-line), reflected (dashed-line) RF-signals and the dark current (dots) with cathode heater off at 3.65 MW with 2 μs (FWHM) RF-pulse width

An additional source of degradation of the RF-gun operation is the dark current which increases when the RF-power increases. It can be seen clearly that the dark current was emitted when the RF-conditioning started and it decreased

as conditioning proceeded. The dark current occurs from the field emission process and is accelerated by the RF-wave. It is only present at the beginning and the end of the RF-pulse, where the field strength is maximum. The dark current was observed at a current transformer downstream from the RF-gun. The total charge emitted from the field emission and forming the dark current is about 7.5 nC with a peak current of 34 mA. Figure 6.1 shows the forward, reflected RF-signal and the dark current without cathode heating at 3.65 MW RF input-power with 2 μs (FWHM) pulse width. The dark current sometimes could even be observed at the current transformer after the α-magnet and at the phosphor screen before the linac entrance. The RF-pulse duration could be shortened to reduce the dark current and to achieve a more stable operation in a higher field gradient. After several hours of RF-conditioning at maximum RF-power without breakdown the vacuum level inside RF-gun improved and the dark current decreased. Generally, RF-conditioning is required the first time the RF-gun was installed into the beamline. However, from our experience the RF-processing of the RF-gun with high RF-power is required every time the gun was opened to poor vacuum because the copper surface is easily contaminated by air and alien material.

6.3 RF-Gun Operation

The RF-gun is a standing wave RF-structure where electrons are generated from a thermionic cathode as part of the gun surface and accelerated in the gun by RF-fields. In PARMELA simulation in Chapter 3 the half-cell and the full-cell have an average electric fields of 23.9 and 45 MV/m, respectively. It gives an electron beam kinetic energy of 2.44 MeV at the RF-gun exit. Scaling with SUPERFISH simulation the electric field gradient at the cathode is 28.8 MV/m. As the RF-fields are excited in the RF-gun the electric accelerating field increases and decreases periodically at the cathode surface. Due to the high field gradient at the cathode some fraction of electrons emitted late in the RF oscillating cycle feel a decreasing RF-fields and do not exit from the gun before the RF-field reverse its direction. These electrons are decelerated back to hit the cathode at high energies. This process is called *electron back-bombardment* and it can be a serious disadvantage of the thermionic RF-gun. These backward electrons hit the cathode and their kinetic energies are transferred to the cathode and heat up the cathode surface significantly causing more electron emission from the cathode

and more back-bombardment effect and so on. The thermionic RF-gun can break down because of these back-bombardment electrons that cannot escape the cavity and hit the cavity wall, resulting in outgassing and generating more electron and ions. The back bombardment effect is the limitation of the thermionic RF-gun. It can cause unstable beam output from the RF-gun and the instability depends significantly on the amount of the external RF-power driving the gun and the cathode heating current from the AC power supply. Some measurements on the electron beam from the RF-gun were performed to study these electron back bombardment. In this section, an external RF-power characteristics was investigated in order to find the optimal condition for the RF-gun operation. Some experimental results will be compared with theory. Observation with a pulsed beam current monitor and an energy measurement instrument provide useful information to establish the desired operating condition to generate an electron beam by adjusting the RF-power pulse length, the RF-power level and the cathode heater power.

6.3.1 Choice of RF-Power

As discussed in Sec.6.2.3, the 6 μs (FWHM) RF-pulse is the maximum pulse length that the RF-gun can handle without the RF-breakdown. However, the longer the RF-pulse the more electron back-bombardment. The RF-pulse duration was shortened in order to reduce the dark-current and the electron back-bombardment effect to achieve a more stable beam operation. From our experience, under RF-gun operation with an RF-pulse longer than 4 μs (FWHM) it was difficult to maintain beam stability. To minimize the electron back-bombardment the RF-pulse width was chosen to be about 2.8 μs (FWHM) by using two capacitors in the pulse forming network (PFN) of the klystron modulator. Figure 6.2 compares the RF-pulse width with 2.8 and 6 μs (FWHM). The rise time of the 6 μs (FWHM) RF-pulse is 2.8 μs before it reaches the point that the beam can be filled with maximum power of about 5-5.2 MW. For an RF-pulse of 2.8 μs (FWHM), the rise time does not even reach the maximum power and thus limiting the peak power to about 3.65 MW. This results in a peak power reduction of $\sim$ 30%. However, the RF-gun operation with a pulse width of 2.8 μs (FWHM) can provide the maximum kinetic energy of about 2.0-2.5 MeV electron beam with a peak current up to 1 A, which is sufficient for our application. Therefore, the RF-pulse width

of 2.8 μs (FWHM) was used in all experiments in this thesis.

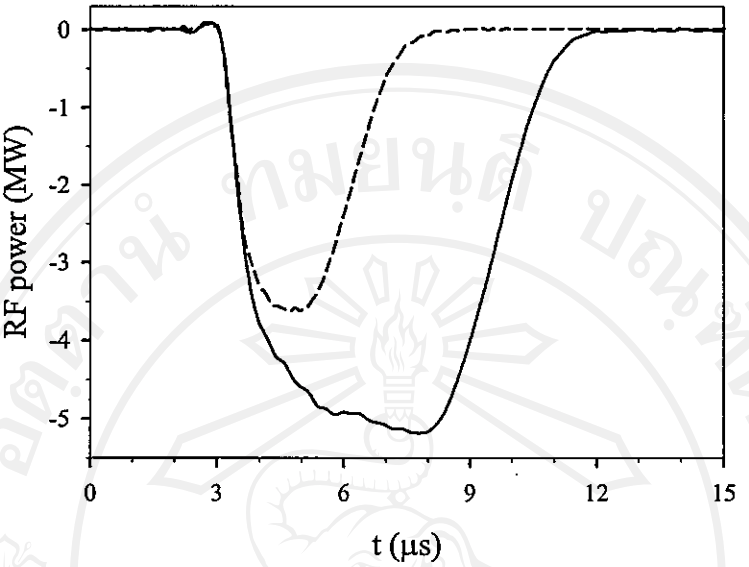

Figure 6.2. Comparison of the RF-pulse with 6 μs (solid-line) and 2.8 μs (dashed-line) FWHM pulse length. The RF-power measurements were performed at 27.5 ^{o}C.

In the first instance the RF-power is turned on all the input power is used to increase the stored energy in the RF-cavity while increasing the dissipated wall losses. The RF-cavity reaches a steady state when the dissipated power equals the input RF-power. The cavity filling time constant in equation (2.56) is used to describe the build up time of the RF-fields in the RF-gun. From the low-power RF-measurement, the unloaded quality factor of our RF-gun is Q_0=12979 and when the RF-gun is operated at 2856 MHz the cavity filling time becomes

$$\tau_U = \frac{Q}{\omega_0} = \frac{12979}{2\pi(2856\ MHz)} \approx 723\ ns. \tag{6.3}$$

The cavity filling time in (6.3) is the time that the cavity needs to build up the stored energy to overcome the dissipated cavity power and the beam loading starts after this filling time.

6.3.2 Forward, Reflected and Absorbed RF-Power

To maximize the stored energy in the RF-cavity and thus the maximum accelerating field strength, the reflected power is needed to be minimized. The

maximum forward RF-power towards the cavity in our case is limited by the breakdown and effect of the electron back bombardment. The waveform signals for the forward and reflected RF-power from the RF-gun were monitored at the directional coupler close to the ceramic RF-window upstream of the RF-gun. The method to measure the RF-power was discussed in Sec.5.5.4. Figure 6.3 presents the measured forward RF-power to the RF-gun cavity (solid line) and the reflected RF-power (dash line) from the RF-gun with cold cathode. The measurement was taken at 27.5°C which is the matched gun temperature obtained from the low-power RF-measurement. Almost all RF-power is reflected, since there is not yet any electron beam.

The shape of the reflected RF-signal can be explained by observing the energy absorption by the RF-gun. The first 600 ns of the RF-power does not match the absorption band of the RF-gun resulting in total reflection by the cavity. The RF-gun starts to absorb after the first 600 ns. It takes about 2.14 μs to reach the position of the most absorbtion occur. Then, the gun cavity starts to reflect again due to de-tuning of the frequency from the klystron central frequency. The maximum stored energy in the cavity and hence the maximum electric field is reached somewhat after the minimum in the reflected power. In case of no electron beam loading, the cavity wall losses of the RF-gun can be calculated from (3.17). From Fig.6.3 we note that the maximum forward RF-power is 3.65 MW and the minimum reflected RF-power is 2.19 MW resulting in the maximum absorbed RF-power by the RF-gun of 1.46 MW.

Moreover, the RF-coupling coefficient (β_{rf}) can be obtained from the measured forward and reflected RF-power as

$$\beta_{rf} = \frac{1 \pm \sqrt{P_r/P_f}}{1 \mp \sqrt{P_r/P_f}}, \tag{6.4}$$

where the plus sign in the numerator and the minus sign in the denominator are used in over-coupled RF-system and vise versa for under-coupled systems. Therefore, the measured RF-coupling coefficient from the high power RF-measurement for the over-coupled RF-system like in our case becomes

$$\beta_{rf} = \frac{1 + \sqrt{2.19/3.65}}{1 - \sqrt{2.19/3.65}} \approx 7.9. \tag{6.5}$$

The RF-coupling coefficient from this high RF-power measurement compares well to the measured value from the low-level RF-measurements by using the network

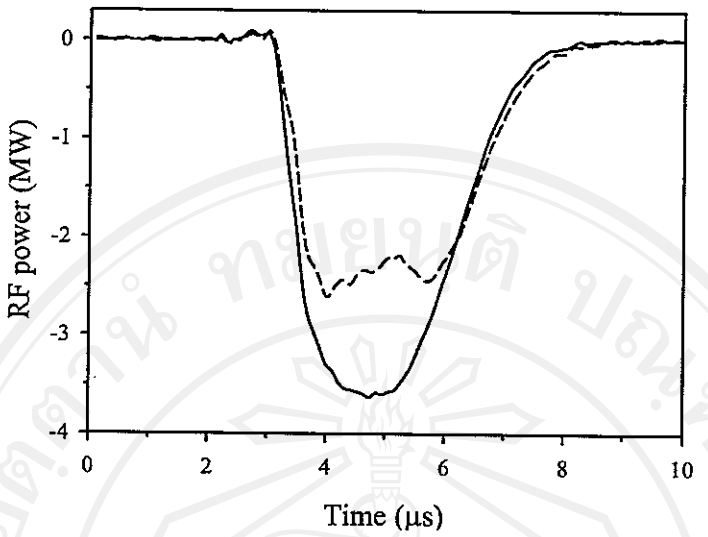

Figure 6.3. Measured forward (solid-line) and reflected (dashed-line) RF-power from the RF-gun for the matched temperature at 27.5°C.

analyzer as described in Sec.4.5.3. The coupling factor β_{rf} derived from the Smith Chart and from VSWR measurement is 7.4 and 7.3, respectively. This RF over coupling will be compensated by beam loading when the cathode heater is on.

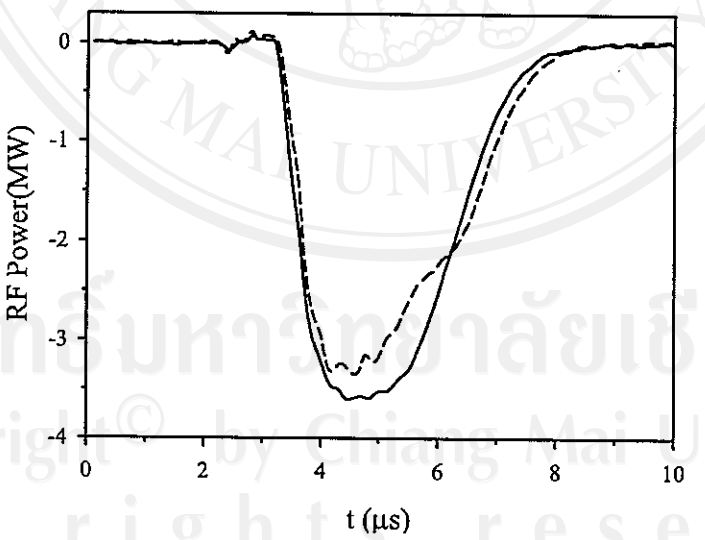

Figure 6.4. Measured forward (solid-line) and reflected (dashed-line) RF-power from the RF-gun at the off-resonance gun temperature at 35°C.

If the RF-gun is operated with a gun temperature far different from the correct value, the RF-gun will not get excited at the resonant frequency of

the klystron. Most of the RF-power will be reflected back from the gun cavity leading to less energy gain. In this case electrons will be accelerated out of the gun with little energy and some fraction of electrons will not even exits the gun. The forward and reflected RF-power in case of a de-tuned gun by temperature is shown in Fig.6.4 while the gun temperature is about 35°C. The increase of gun temperature of 7.5 °C leads to a decrease of resonant frequency by about 362 kHz (-48.3 kHz/°C). It can be seen from Fig.6.4 that there is only little power absorption at the end of the RF-pulse and the reflected RF-power becomes larger than the forward power at about 200 ns at the end of the pulse. Because of the high Q of the gun a frequency shift of 362 kHz shifts the excitation off the resonance curve and virtually no field can be generated in the gun cavity.

6.4 RF-Gun and Electron Beam Characterization

At the SURIYA facility, the RF-gun is operated at 2856 MHz and the thermionic cathode is heated through a filament by an AC power supply. Since the electron back-bombardment depends on the RF-fields cycle, which change cyclicly in time as the RF-power is fixed at a certain level adjusting of the cathode heating is necessary to maintain stability of gun operation and also beam output stability. Presently, this cathode heating adjustment is made manually and the stability of the beam is not as good as required. The beam instability affects the quality of the beam and specially the production of the transition radiation, which will be described in Chapter 7. A cathode feedback control by computer is required to maintain stable RF-gun operation. The self-heating of the cathode from back-bombardment is greatly affected by the current amplitude, pulse length and energy of electron beam. More details of this effect will be discussed physically and experimentally in the this section.

6.4.1 Electron Beam Generation

All measurements shown in this chapter were obtained by operating the RF-gun at 3.65 MW with 2.8 μs (FWHM) RF-pulse width at a repetition rate of 10 Hz. The cathode heating power was varied between 13-16 W to give a the cathode temperature of 950-1000 °C while the RF-gun temperature was kept at 27.5 °C. The electron beam pulses generated from the gun have a pulse width of about

1-2.5 μs depending on the cathode temperature. These electron pulses are called macropulse, containing about 3000-7000 microbunches. Not all microbunches are identical within a macropulse since they are distributed along the pulse with different energy gain from the variety RF-pulse.

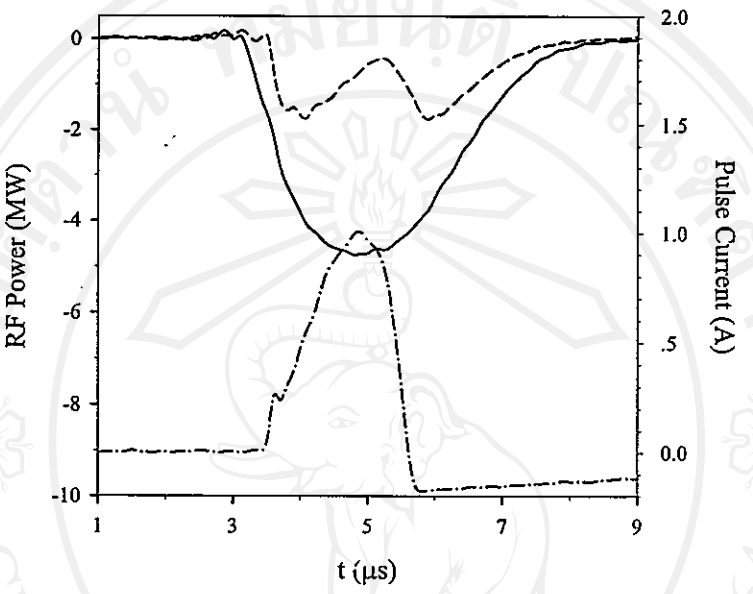

Figure 6.5. Waveforms of the forward (dashed-line), reflected (solid-line) RF-pulses and the typical electron pulses at the RF-gun (bottom curve). Theses waveforms were observed when the cathode power is 13.62 W (~950 °C).

The electron macropulses generating from the RF-gun were observed at the current transformer CT1 after the gun exit. The signal from the current transformer was observed by an oscilloscope and represents the macropulse current. Figure 6.5 shows waveforms of the forward, reflected RF-power and the macropulse current (CT1) for a cathode heating power of 13.62 W. Because the RF-gun is a standing-wave RF-structure it reflects the RF-power at the beginning and at the end of the RF-pulse as shown in Fig.6.5. The actual electron pulses exit the RF-gun with a very large energy spread. The α-magnet includes energy slit to select the desired energies of the electrons or to reduce the macropulse length.

Electron macropulse generated from the thermionic RF-guns has a triangular pulse shape with slower rising time than the falling time (see in Fig.6.5). The steeper edge at the end of the pulse shows that the cathode is heated and emits more electrons. This is the sign of electron back-bombardment which cre-

ating a large amount of electron which do not gain much energy anymore. These low energy electrons are lost before they reach the CT1, this simulating a sharp decrease of the pulse. The peak of the triangle represents the maximum current with maximum energy occurring when the RF energy at that point of the RF-pulse is mostly consumed by the beam. When there is beam loading in the RF-gun the forward RF-power increases from 3.65 MW to about 4.4 MW. It was thought that it might because of the coupling coefficient of the directional coupler error. However, it was not clear that what is the real reason. The absorbed RF-power calculated from the waveforms in Fig.6.5 is about 4.19 MW. The kinetic energy of the electron measured by the α-magnet energy slits and the peak current measured at CT1 are about 2 MeV and 1 A, respectively. These values lead to a beam power of $P_b \approx I_b \times E_{kin} = 2$ MW. As discussed in section 6.3.2, the wall losses of the RF-gun are 1.46 MW, then $P_{cy} + P_b \approx 3.46$ MW, which is comparable to the incident RF-power from the klystron of 3.65 MW.

6.4.2 Beam Loading and Electron Back bombardment

When beam operation starts a macropulse current is generated from the RF-gun. The cathode heater voltage is set initially at about 7 V for a few minutes, which results in a heater power of roughly 16-16.5 W or cathode temperature of around 1000-1010 °C, to extract electrons from the cathode surface. The cathode heater voltage must then be slowly decreased to a normal operating point at around 3 V or 13.5 W (950 °C) when the desired beam output is obtained. The cathode heater may need to be adjusted regularly to maintain the beam at the desired intensity. The beam current produced from the RF-gun can be increased by raising the cathode heater power. However, while the cathode temperature increases electron back bombardment usually occurs. This effect causes the beam current to increase quickly and results in a reduction of the accelerating electric field due to the beam loading. An increase of beam current correspond to a change in RF-power coupling to the RF-gun. Less RF-power is coupled into the gun and the electric field is smaller. The reflected power increases at the tail of the macropulse again due to falling beam current and less than optimum coupling. It leads to less electron current output and lower electron energy. Moreover, the additional electron back bombardment current to the cathode surface can cause more electrons to be emitted resulting in more beam loading and further

reduction of the electric field. Although, the electron emission is increased back-bombardment leads to less and less beam output resulting in shortening of the beam pulse and broadening of the energy spread. Hence, the back-bombardment phenomenon is the limitation of the macropulse duration and output current. The beam pulse shortening phenomena in an electron RF-gun was reported clearly by Y. Huang [61]. The results of our experiments concerning back bombardment is presented and discussed in this section.

6.4.3 Cathode Temperature Effect

The current and energy of electron bean generated from the RF-gun depends significantly on the cathode temperature. The cathode temperature is required to be optimized in order to produce the electron beam within the useful limit. To optimize the operating cathode temperature, observations of beam loading for different cathode temperatures and various RF excitation were conducted. Since the cathode surface cannot be observed directly when the RF-gun is in operation the cathode temperature is monitored through the cathode filament resistance and power. The cathode temperature can be obtained from the cathode test results by the Pyrometric measurement presented in Chapter 4 (Fig.4.7).

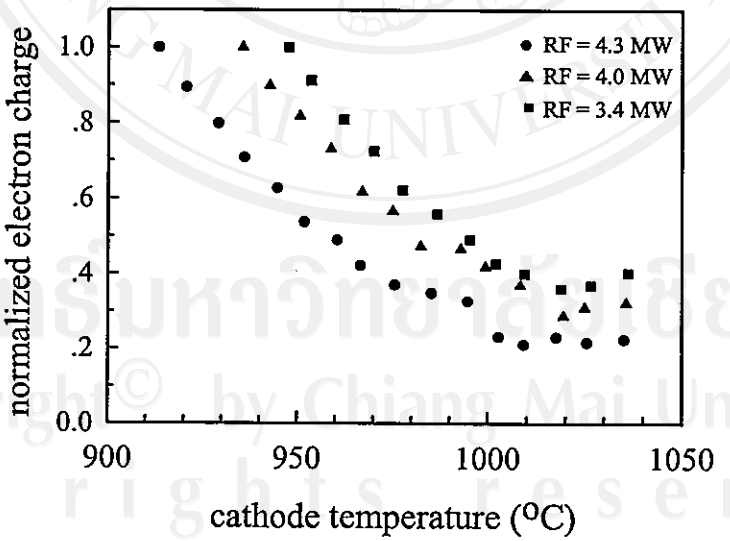

Figure 6.6. Normalized electron charge from the RF-gun as function of cathode temperature for diffident RF-power levels.

The study of cathode temperature effects on electron charge was performed and the results are presented in Fig.6.6 for three different RF-power levels;

3.4, 4.0 and 4.3 MW. The observations reveal that the cathode has to be heated to reach a temperature threshold where electrons can be emitted. The cathode temperature threshold for the RF-power of 3.4, 4.0 and 4.3 MW is 950 °C, 940 °C and 910 °C, respectively. At a temperature lower than the limit no electron will be emitted. On the other hand, heating the cathode to a temperature above the limit will lead in current saturation due to electron back-bombardment. The study results also show that for higher RF-power employed to the RF-gun lower cathode heating is needed. However, the higher the RF-power the higher in electron back bombardment effect and a compromise must be made. Operation with a peak RF-power of about 3.0-4.5 MW, the RF-gun can produce an electron beam with a peak beam current of about 200 mA to over 1 A.

Observations of the electron pulses for different cathode heating power under fixed RF-power at 3.65 MW were performed to investigate the beam loading phenomena. The energy slits inside the α-magnet vacuum chamber was used to measure the maximum kinetic energy of the electron beam at various cathode temperatures. The electron beam current and its pulse length were detected at the current transformer (CT1) after the gun. The beam current, beam pulse length and beam energies are plotted as functions of the cathode heating power reflecting the cathode temperatures. Results of theses observations are shown in Fig.6.7 and Fig.6.8.

It can be seen in Fig.6.7 and Fig.6.8 that the amount of electron current exiting the RF-gun depends greatly on the cathode temperature. There is some threshold temperature below which no electrons are emitted from the cathode and some temperature above which saturation occurs. As the cathode heating power was increased from 13 W to 16.5 W, the beam macropulse width decreases from 2.8 μs to 1 μs. The maximum kinetic energy of the beam also reduces from 2.6 MeV to 0.5 MeV. The observation results in Fig.6.8 show that the beam peak current increases quickly up to 1 A when the cathode heating power was set at 13.1-13.2 W and it stays stable at 1 A until the heating power was raised to 14.2 W and drop to about 900 mA when the cathode heating power was further increased. However, the beam macropulse width became shorter than 1.8 μs when the cathode temperature was raised above 13.2 W. Results of these observations reveal that to achieve a electron pulses of about 2.0-2.5 μs with maximum kinetic energy of 2.0-2.6 MeV at the beam peak current of 1 A the cathode heating power should be kept around 13.1-13.2 W or at about 950°C. However, the cathode temperature

cannot be kept at a constant value due to the electron back-bombardment effect and needs to be adjusted constantly during the beam operation.

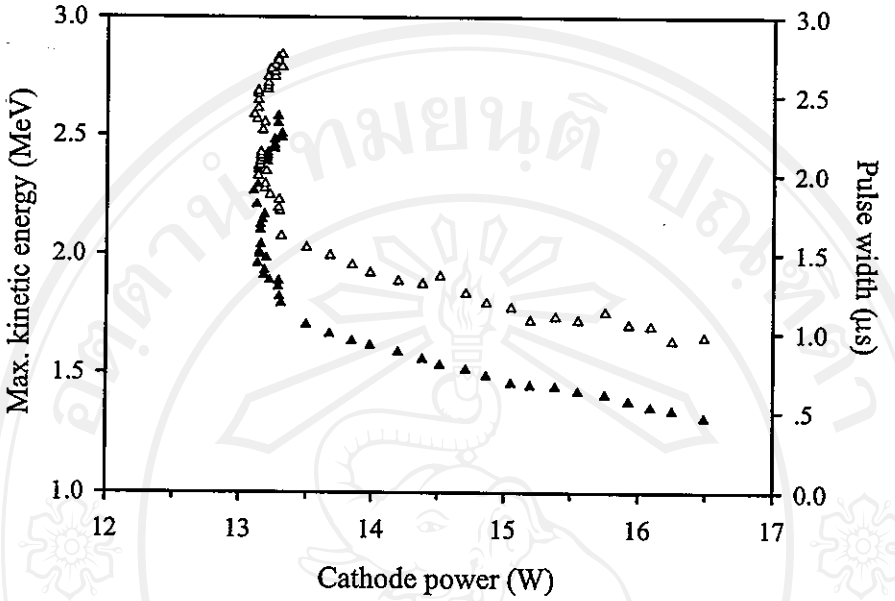

Figure 6.7. Maximum kinetic energy (black triangle) of electron beam and the beam pulse width (white triangle) as a function of cathode heating power.

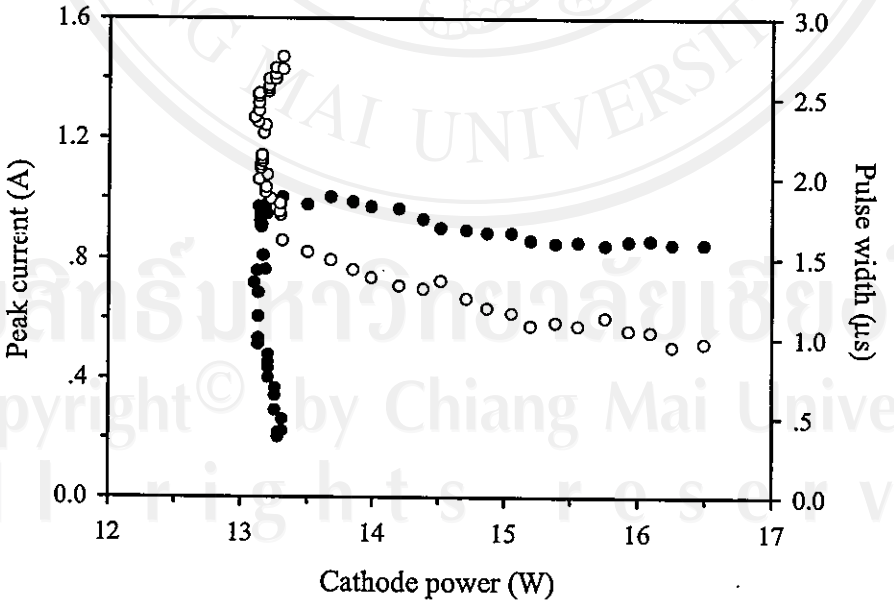

Figure 6.8. Beam peak current (black dots) and the beam pulse width (white circles) as a function of cathode heating power.

6.4.4 Beam Current and Energy

The beam current pulses at different cathode heating power are shown in Fig.6.9 to Fig.6.11 (left). It can be seen that as the cathode power or cathode temperature increases the minimum reflected RF-power point moves to the left of the graph. The peak of the current pulses also moves with the minimum reflected RF-power position. This evidence confirms that most energy is absorbed at minimum reflected RF-power. These three cathode temperatures represents three cathode operating conditions: cold, middle and warm cathode temperature. As the cathode temperature increased at a fixed RF-power, the beam current increase, but the energies and the current pulse length decrease as listed in Table 6.1.

Table 6.1. Electron beam parameters at different cathode heating powers.

Cathode operating condition	cold	middle	warm
Cathode temperature (W)	13.41	13.62	13.97
Cathode temperature (°C)	945	950	959
Max. kinetic energy (MeV)	2.01	1.98	1.87
Macropulse length (μs)	2.3	2.1	1.9
Electron charge (μC)	1.29	1.36	1.28
Beam peak current at CT1 (A)	0.88	1.01	1.04
Beam peak current at CT2 (mA)	297	385	358

We measured the energy spectrum of the electron beam at three different cathode temperatures as shown in Fig.6.9-Fig.6.11 (right) by moving the high energy scraper in steps of 0.05 MeV while the low energy slit was fixed at 0.6 MeV. The results show that for the middle cathode temperature a large portion of electrons has high energies with the number of electron per energy bin exceeding 2.0×10^{11} electron per bin at energies of 1.5-2 MeV. This is quite good for selecting a useful fraction of electron with high energies for further acceleration in the linac. For a cold cathode, the maximum kinetic energy that can be obtained is the highest among the three cases but electrons are not bunched at the high energy bin. For the warm cathode, the beam energies were low and the electrons are distributed almost uniformly over an energy rage of 1-1.8 MeV. The precision of this measurement was limited by the inefficiency of the energy slits since the energy slits work perfectly according to equation (5.1)-(5.3) only for ideal electrons

which are on-axis and enter the α-magnet with zero divergence. Some undesirable electrons may be included in the selected energy bin and some desired electron energies may be lost due to their large angles or displacement from the energy slits. The effect of the unperfect energy measurement can be found in reference [62] and needs to be studied more experimentally.

From our experience, to operate the RF-gun at the middle cathode temperature was the most stable condition. It was not required to adjust the cathode temperature as often as under the cold cathode condition. There was also stable operation for a warm cathode but the beam output from the warm cathode was not useful as the electron energies are low, the beam pulse was shorter than 2 μs and electrons are not bunched at the high energy bin. Because of this pulse shortening and the energy lowering, we normally avoid to operate the RF-gun at a hot cathode temperature. The ripple of the number of electron per bin at the peak of the energy spectrums may come from the instability of the electron pulses during measurements.

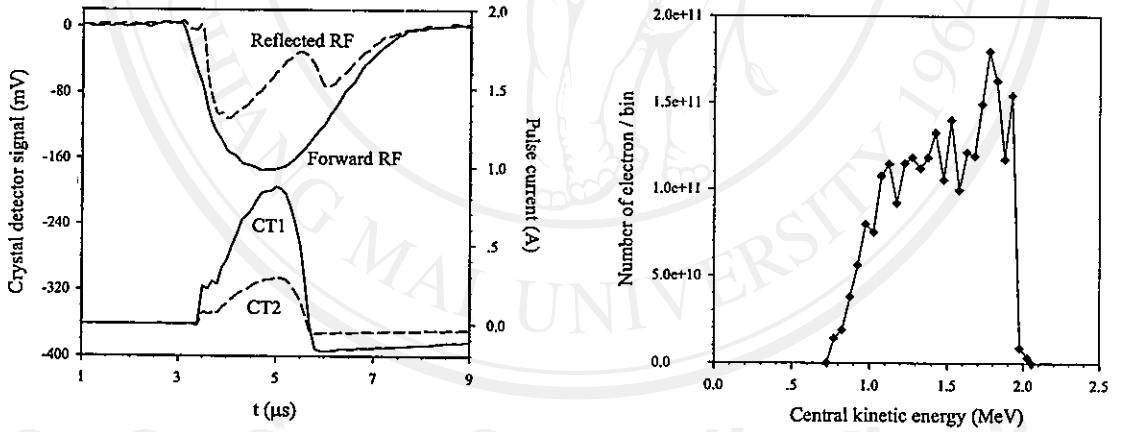

Figure 6.9. RF-pluses and electron pulse currents (left) and energy spectrum (right) when the cathode heater power of 13.41 W (945°C).

6.4.5 Beam Profile Measurements

A *Beam profile* or the particle beam intensity distributions is divided into two categories; the transverse and the longitudinal beam profile. The longitudinal beam profile determines the longitudinal intensity distribution resulting in the bunch length. The transverse beam profile displays transverse distribution

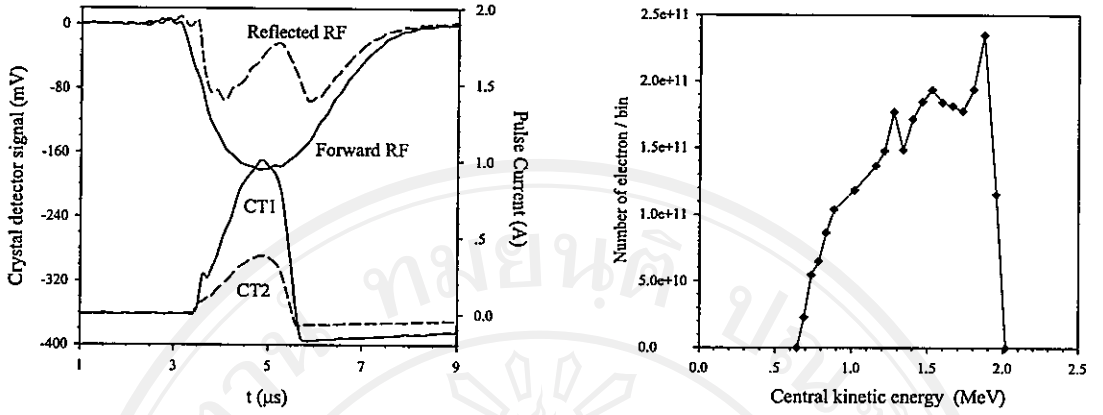

Figure 6.10. RF-pluses and electron pulse currents (left) and energy spectrum (right) when the cathode heater power of 13.62 W (950°C).

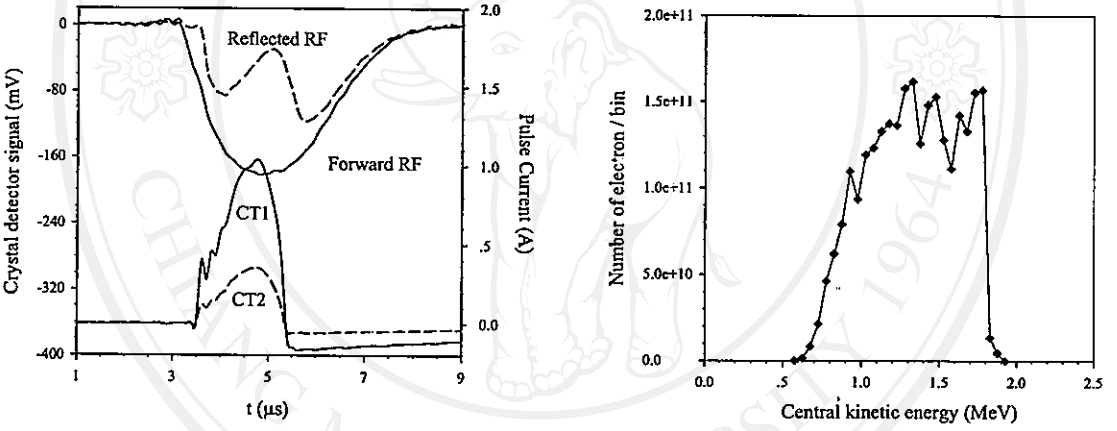

Figure 6.11. RF-pluses and electron pulse currents (left) and energy spectrum (right) when the cathode heater power of 13.79 W (960°C).

of the particle beam and its envelope determines the transverse beam size. The transverse beam profile is monitored with phosphor screens and the image captured by a computer. The phosphor screen is illuminated by the collided electron beam with the image intensity proportional to the particle density. The actual size of the beam projected on the screen can be calculated with the calibration conversion of the captured image size and the real size.

The beam profile measurement for the output beam from the RF-gun taken at SURIYA followed the method described in reference [55] and in Sec.5.6.2. Figure 5.10 shows an image of 2.5 MeV (total energy) electrons on the phosphor screen, which was placed in the beamline at about 43 cm before the linac entrance,

and the relative intensity at the screen for 2D-profile and the 3D-distribution. The horizontal and vertical profiles present the beam intensity distribution of the image and they are the cross-section through the beam core where the most intense part appears. Each profile has a shape similar to a bell-shape. By fitting the beam profile to a Gaussian, the standard beam size parameters (σ_x, σ_y) determined at FWHM of these profiles are obtained. Results of the beam profile measurement reveal that the actual size of the beam is σ_x =3.1 mm and σ_y =3.4 mm in x and y axis, respectively.

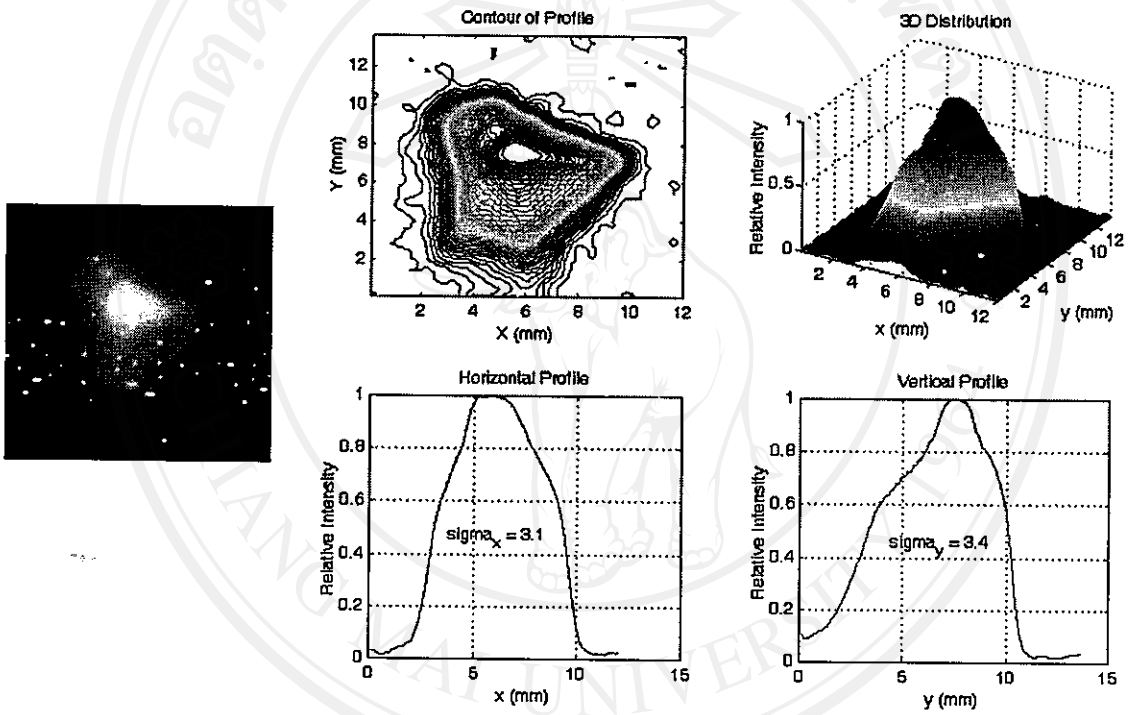

Figure 6.12. 2.4 MeV electron beam image (left), the relative intensity distribution of electron beam in two and three dimension and the horizon and vertical beam profiles.

6.5 Electron Beam Acceleration from Linear Accelerator

An electron beam with 2.7 MeV total energy was further accelerated by the SLAC-type linac after bunch compression in the α-magnet. The linac is a section of the SLAC linac structure with a length of 10 ft (3.048 m) and was used to accelerate the electron beam for the Stanford SUNSHINE system. The acceleration of the linac depends on the input RF-power as can be seen from

equation (5.4). Measurements of the forward and reflected RF-power of the linac at SURIYA were performed and the results are shown in Fig.6.13. The results show that the 6.4 MW RF-power of 8 μs (FWHM) pulse width with 4-5 μs flat top is available. Generally, the reflected RF-power should not be present in a linac since it is a travelling wave RF-structure. However, a reflected RF-power of about 1.3 MW appears in our measurements. This may come from the de-tuned condition of the linac or the mismatch of the input RF-frequency from the klystron and the resonant frequency of the linac. The linac temperature should be adjusted in order to bring the resonant frequency of the linac to match with the klystron frequency. Another reason may come from the coupling error of the diagnostic port of the directional coupler where the measurement take place. However, from measurement results the transmitted RF-power can be calculated to be 6.35-1.25 = 5.1 MW. Calculation of the linac acceleration from (5.4) with 5.1 MW input RF-power yields to a maximum energy gain of

$$\Delta E_{kin}[MeV] = 10.48\sqrt{5.1[MW]} \approx 23.7\ MeV. \tag{6.6}$$

This energy gain is the possible maximum acceleration that the SURIYA system can provide with the available RF-power without including the beam loading effect. The maximum linac acceleration in this case becomes 7.8 MeV/m.

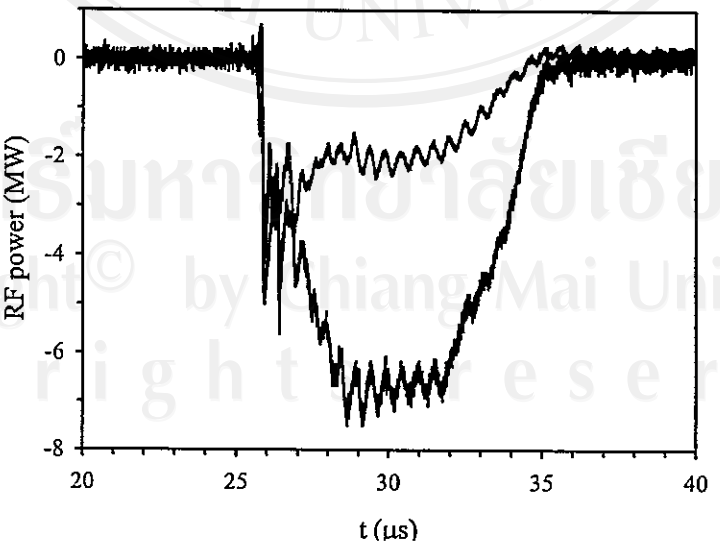

Figure 6.13. Waveforms of the forward (bottom curve), reflected (top curve) RF-pulses of the linac at typical linac operation at 45 °C.

When there is a beam loading in the linac, the total accelerating voltage is reduced due energy extraction from the fields by the beam of current i_b and leads the maximum energy gain of [28]

$$\Delta E_{kin}[MeV] = 10.48\sqrt{5.1[MW]} - 37.47 i_b[A]. \tag{6.7}$$

To measure energy and current of the electron beam before the linac acceleration, the low energy scraper of the α-magnet energy slit was fixed at the minimum kinetic energy of 1.75 MeV with the α-magnet gradient of 396.7 G/cm. The maximum kinetic energy of the electron beam before the linac acceleration in this case was 2.24 MeV. Hence, the central kinetic energy of the input beam for the linac was about 2 MeV with energy spread of about $\pm 11\%$. An input electron beam current for the linac was measured at the current transformer after the α-magnet exit (CT2). The current measurement result shows that the electron beam enters the linac with current of about 170 mA. Thus, the maximum energy gain from linac section calculating from (6.7) for this beam loading condition should be 17.3 MeV

The electron beam energy after the linac acceleration was measured by using a dipole magnet at the end of the beam transport line (as described in Sec.5.6.3). Beam energy measurements were performed by observing the beam image on the phosphor screen after the beam was deflected 60^o from the dipole field. The dipole magnet functions as a bending element, electrons with different energies follow different trajectories. Therefore, the electron beam energy can be measured by bending the beam and observing the beam image as a function of magnetic field (or as a function of excitation current) at a fixed bending angle. A phosphor screen was inserted after the dipole magnet vacuum chamber and used to monitor the beam image and infer the beam energy by computer code *Trajectory Simulator* [60].

The energy measurements reveal that so far the 2.8 MeV (total energy) electron beam from the RF-gun was accelerated to about 11.2 MeV, thus the kinetic energy gain from the linac was 8.4 MeV leading to a linac acceleration of 2.7 MeV/m. This linac acceleration is about 50% less than the calculation value from (6.7). As the RF-phase in the linac change the maximum energy gain of the electron beam changes as well. The RF-phase of the linac must be optimized to provide maximum energy gain and minimum energy spread of the beam. Future

optimizations are required to optimize the RF-phase in the linac with respect to the RF-phase from the RF-gun by adjusting the RF-phase shifter (as described in section 5.5).

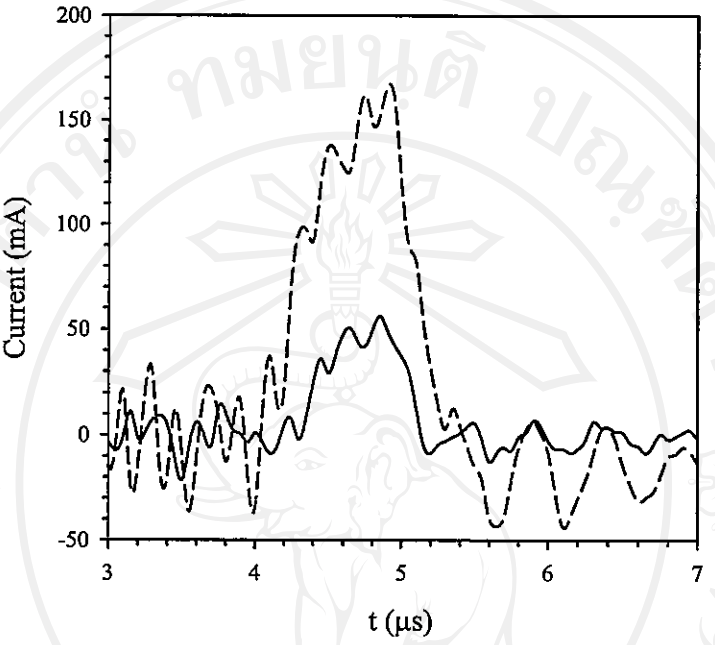

Figure 6.14. Beam pulse current measured at CT2 after bunch compression (dash line) and at CT3 after the linac acceleration (solid line).

The electron beam current that can be accelerated was observed at the current transformer downstream of the linac (CT3). The waveforms of the beam pulse before and after the linac are shown in Fig.6.14. The measurement of the beam current after linac acceleration shows that the electron beam current of 170 mA with 1.3 μs pulse length is reduced to about 50 mA with 0.8 μs long after the linac acceleration. The number of electron in the beam pulse reduces from 7.4×10^{11} to 1.88×10^{11}. There is about 75% loss in the linac. This evidence confirms the improper RF-phase in the linac as well as the mismatch of beam focusing and steering causing a significant losses.

Optimization of the linac RF-phase and the beam focusing and steering is required in order to accelerate more electron current through the linac with higher energy gain. The linac beam current and energy instability usually coincides with the change in the temperature of the RF-gun cathode. Just a little change in the beam pulse waveform at CT1 results greatly at the beam output from the linac

as observed at CT3. This also results in the sensitivity of the beam current at the transition radiation which will discussed in Chapter 7.

6.6 Conclusion of Electron Beam Characteristics at SURIYA

It can be concluded at the end of this chapter that a 2.5-3 MeV electron beam with a peak current up to 1 A (8×10^{12} electrons/macropulse) can be produced from the RF-gun. Roughly 50-60% of the electron current from the gun is filtered out by the α-magnet energy slit depending on the α-magnet field gradient. The beam generating from the RF-gun consists of electron macropulses approximately 2 μs long at a repetition rate of 10 Hz. Within a macropulse, there is a train of about 5700 microbunces with each bunch separated by 350 ps corresponding to the RF-frequency (2856 MHz). Each microbunch consists of about 1.4×10^9 electrons. From the definitions of electron current in Chapter 1, the total electric charge per bunch can be derived as $q_{bunch} = (1.4 \times 10^9)(1.602 \times 10^{-19}) = 0.22$ nC. The pulse current can be calculated as $I_{pulse} = (2.2 \times 10^{-10})/(350 \times 10^{-12}) = 628.6$ mA and for the average current , it will be $I_{ave} = (5700)(2.2 \times 10^{-10})/(100ms) = 12.5$ μA.

Table 6.2. Typical operating parameters and electron beam characteristics at SURIYA facility (April 2006).

Parameters	RF-gun	Linac
Resonant frequency (MHz)	2856	2856
Repetition rate (Hz)	~10	~10
Input RF-power (MW)	3.65	6.35
Max. beam energy (MeV)	2.5-3	11.1
Beam peak current (mA)	1000	50
Macropulse length (μs)	2	0.8
Number of bunches per macropulse	5700	2300
number of electrons per bunch	1.4×10^9	8.2×10^7

After the beam was accelerated through the linac, the output beam macropulse length reduces to about 0.8 μs with 1.9×10^{11} electrons. Within a macropulse, there is a train of about 2300 microbunces with 350 ps separation. Each microbunch consists of 8.2×10^7 electrons. Similarly, the total electric charge

per bunch can be derived as $q_{bunch} = (8.2 \times 10^7)(1.602 \times 10^{-19}) = 13.1$ pC. The pulse current can be calculated as $I_{pulse} = (1.31 \times 10^{-11})/(350 \times 10^{-12}) = 37.5$ mA and for the average current, it will be $I_{ave} = (2300)(1.31 \times 10^{-11})/(100ms) = 0.3$ μA. Typical operating parameters and the electron beam characteristics at SURIYA facility are listed in Table 6.2.